NEUROPHOTONICS

RESEARCH PAPER

Cerebral baseline optical and hemodynamic properties in pediatric population: a large cohort time-domain near-infrared spectroscopy study

Valeria Calcaterra[a,b,†] Michele Lacerenza,[c,†] Caterina Amendola,[d] Mauro Buttafava,[c] Davide Contini,[d] Virginia Rossi,[a] Lorenzo Spinelli,[e] Sara Zanelli,[a] Gianvincenzo Zuccotti,[a,f] and Alessandro Torricelli[d,e,*]

[a]Buzzi Children's Hospital, Pediatric Department, Milan, Italy
[b]University of Pavia, Pediatric and Adolescent Unit, Department of Internal Medicine, Pavia, Italy
[c]PIONIRS s.r.l., Milan, Italy
[d]Politecnico di Milano, Dipartimento di Fisica, Milan, Italy
[e]Consiglio Nazionale delle Ricerche, Istituto di Fotonica e Nanotecnologie, Milan, Italy
[f]University of Milan, Department of Biomedical and Clinical Science, Milan, Italy

ABSTRACT. **Significance:** Reference cerebral near-infrared spectroscopy (NIRS) data on the pediatric population are scarce, and in most cases, only cerebral oxygen saturation (SO_2) measured by continuous wave spatially resolved spectroscopy NIRS is reported. Absolute data for baseline optical and hemodynamic parameters are missing.

Aim: We aimed at collecting baseline cerebral optical parameters [absorption coefficient, μ_a; reduced scattering coefficient, μ_s'; differential pathlength factor (DPF)] and hemodynamic parameters [oxy-hemoglobin content (HbO_2), deoxyhemoglobin content (HHb), total hemoglobin content (tHB), SO_2] in a large cohort of pediatric patients. The objectives are to establish reference optical values in this population and evaluate the reproducibility of a commercial time domain (TD) NIRS tissue oximeter.

Approach: TD NIRS measurements were performed in the prefrontal cortex at 686 and 830 nm with a 2.5-cm source–detector distance and 1-Hz acquisition rate. Five independent measurements (after probe replacement) were taken for every subject. TD NIRS data were fitted to a photon diffusion model to estimate the optical parameters. From the absorption coefficients, the hemodynamic parameters were derived by Beer's law. Auxological and physiological information was also collected to explore the potential correlations with NIRS data.

Results: We measured 305 patients in the age range of 2 to 18 years. Absolute values for baseline optical and hemodynamic parameters were shown as a function of age and auxological variables. From the analysis of the repositioning after probe replacement, the time-domain near-infrared spectroscopy device exhibited an average precision (intended as coefficient of variation) of <5% for μ_s', DPF, HbO_2, HHb, and tHb, whereas precision was <2% for SO_2.

Conclusions: We provided baseline values for optical and hemodynamic parameters in a large cohort of healthy pediatric subjects with good precision, providing a foundation for future investigations into clinically relevant deviations in these parameters.

 [DOI: 10.1117/1.NPh.11.4.045009]

*Address all correspondence to Alessandro Torricelli, alessandro.torricelli@polimi.it

†These authors contributed equally to this work.

Keywords: optical properties; hemodynamic properties; pediatric population; healthy; baseline; reproducibility

Paper 24049GRR received Jun. 13, 2024; revised Oct. 18, 2024; accepted Oct. 22, 2024; published Nov. 15, 2024.

1 Introduction

The ability of red and near-infrared light (~650 to 1000 nm) to diffuse into human tissues has fostered the development of a plethora of optical techniques to noninvasively study human brain functions and diseases.[1] Near-infrared spectroscopy (NIRS) was initially introduced to monitor cerebral oxygen saturation (SO_2) in children and adults at the bedside by exploiting the different absorption spectra of oxygenated and deoxygenated hemoglobin.[2,3] Later, functional NIRS took advantage of the neurovascular coupling mechanism, such as in functional magnetic resonance imaging, to provide a complementary tool to study human brain mapping in ecological settings.[4–6] More recently, diffuse correlation spectroscopy (DCS), speckle contrast optical spectroscopy (SCOS), and interferometric NIRS completed the hemodynamic description by adding valuable information on cerebral perfusion and metabolism.[7]

Neonates, infants, and children, having thinner skulls than adults, show reduced light attenuation and enhanced light penetration; therefore, they represent the ideal target population for probing the brain through noninvasive optical techniques. Nonetheless, several studies are currently performed also on adults. The incessant growth of these optical techniques and their adoption in biomedical and clinical applications has been supported by the availability of guidelines for best practice and (open source) data analysis tools[8,9] and by the parallel advance in modeling light propagation in diffusive media.[10,11]

Although for several applications the measurement of trends, or relative changes with respect to a baseline (in arbitrary units), might be sufficient (e.g., when studying the hemodynamic response function following a stimulus or the perfusion changes during a bed tilt test), the knowledge of the absolute baseline values for the quantities of interest is crucial when it comes to quantifying those changes in view of a more accurate and robust assessment of the response.

Aiming for quantitation, the knowledge of tissue optical properties (absorption coefficient, μ_a, and reduced scattering coefficient, μ_s') is fundamental because it enables accurate modeling of light propagation in complex heterogeneous structures (such as the human head) and the investigation of specific features of the optical techniques (e.g., depth penetration, depth sensitivity, signal-to-noise ratio, and contrast-to-noise ratio).

In the literature, several studies report optical properties of neonates[12–20] and adults,[21–32] whereas very few focus on the pediatric population with also a limited number of measured subjects.[33–36] NIRS data on population in pediatric age in the majority of cases refer only to SO_2, as measured by continuous wave (CW) spatially resolved spectroscopy NIRS devices, whereas absolute data for baseline optical and hemodynamic parameters are missing.[37]

The aim of this work is to collect baseline cerebral optical parameters [absorption coefficient, μ_a; reduced scattering coefficient, μ_s'; and differential pathlength factor (DPF)] and hemodynamic parameters [oxy-hemoglobin content (HbO_2), deoxyhemoglobin content (HHb), total hemoglobin content ($tHb = HHb + HbO_2$; $SO_2 = HbO_2/tHb$)] in a large cohort of pediatric patients in the age range of 2 to 18 years. The primary objective is to establish reference optical and hemodynamic values in this population, whereas a secondary (but equally important) objective is to evaluate the reproducibility of a time domain (TD) NIRS tissue oximeter.

2 Material and Methods

2.1 Subjects

The study was conducted from March 2023 to February 2024 at Buzzi Children's Hospital (Milan, Italy) on a pediatric cohort of healthy subjects in stable conditions. The following inclusion criteria were considered: absence of fever, absence of cardiac or pulmonary pathologies, no chronic diseases, no ongoing pharmacological treatments, stable vital parameters [heart rate (HR), respiratory frequency (BR), and peripheral oxygen saturation (SpO_2)], absence of wound

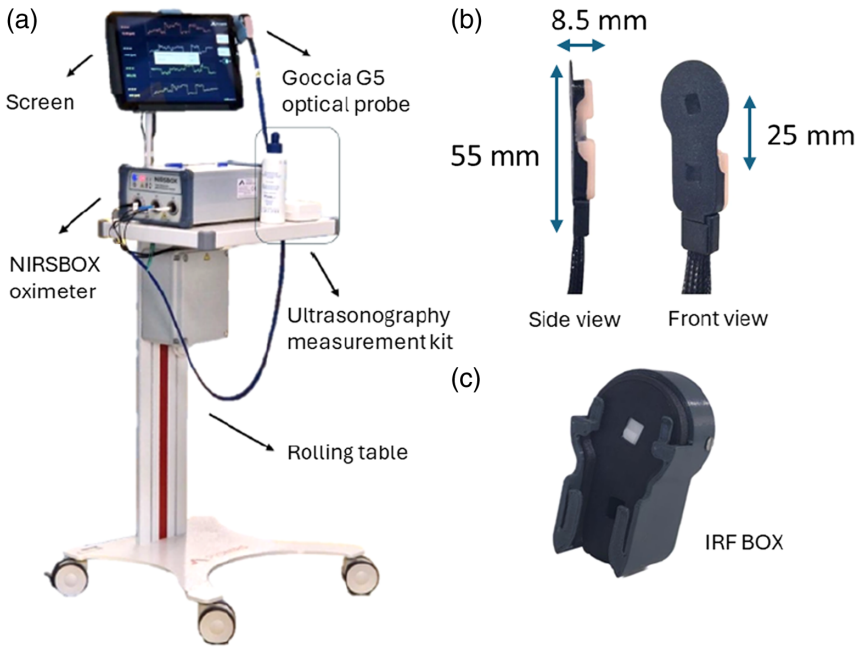

Fig. 1 (a) NIRSBOX tissue oximeter, as used in the clinical environment (cart-mounted configuration). (b) G5 Goccia probe. (c) IRF box.

in the measured position, and confirmation of normal hematocrit levels through blood analyses. The study was conducted in accordance with the Helsinki Declaration of 1975, as revised in 2008. The institutional ethics committee approved the protocol (Ethics Committee Milano Area 1; Study Registration 2022/ST/229; Protocol No. 0004021/2023 Date 30/01/2023). After receiving information about the study, all participants, or their guardians, provided written consent.

2.2 Time-Domain Near-Infrared Spectroscopy (TD-NIRS) Device

A commercially available, research-grade, tissue oximeter, NIRSBOX (PIONIRS s.r.l., Milan, Italy), based on TD-NIRS technology was used (see Fig. 1).[38] The device employs proprietary picosecond diode lasers emitting at 686 and 830 nm, along with a single-photon detector (silicon photomultiplier, with optical filters to reduce ambient light noise) and timing electronics (time-to-digital converter, with a 9.7-ps/ch resolution) to record the distribution of time-of-flight (DTOF) for the photons re-emitted from the tissue. The NIRSBOX device is battery-operated (7-h lifetime) and hosted in a compact, four-wheel medical grade chart equipped with a 13-in. screen. In this study, the G5 Goccia optical probe (PIONIRS s.r.l., Milan, Italy) was employed, characterized by a single channel with a source–detector distance $\rho = 2.5$ cm and a built-in capacitive contact sensor to ensure accurate application on the tissue and secure enablement of laser emission. The probe is flexible, waterproof, and undergoes sanitation with isopropyl alcohol among each patient. To acquire the instrument response function (IRF), the probe is positioned into the PIONIRS IRF box.[39]

2.3 Protocol

Measurements were performed on the left prefrontal cortex (Fp1 position of the 10/20 International System Mapping), targeting cerebral optical properties and hemodynamic parameters. The protocol included the acquisition of five DTOFs at a 1-Hz acquisition frequency. Then, other four identical measurements were performed after probe replacement (i.e., removing the probe from the tissue, placing the probe again in contact with the tissue, and acquiring data). Overall, 25 DTOFs were acquired (five replacements times five DTOFs/replacement) from each subject. The optical probe was manually held in place by the clinical operator during measurement and kept in hand during probe removal and probe replacement. The entire measurement protocol took ~2 min per subject. To assess a child's growth and physical development, in all

children, auxological measurements including weight, height, body mass index (BMI), and head circumference were recorded. BMI values were calculated as body weight (kg) divided by squared height (m^2) and then standardized into BMI z-scores according to the reference values obtained from the World Health Organization database,[40] specifically "BMI-for-age 2 to 5 years" and "BMI-for-age 5 to 19 years."[41,42] In addition, following the usual clinical practice, HR, BR, and SpO_2 were measured by standard clinical grade devices, whereas hematocrit percentage (HTC) and hemoglobin concentration (Hb) were obtained by venous sample.

2.4 Data Analysis

The solution of the photon diffusion equation for a semi-infinite homogeneous medium with extrapolated boundary conditions was used[43] (after convolution with the IRF) to retrieve from each measured DTOF the optical properties (absorption coefficient, μ_a, and reduced scattering coefficient, μ_s') of the tissue under investigation. Then, from each DTOF, the DPF was calculated as $\mathrm{DPF}(\lambda) = v\langle t(\lambda)\rangle/\rho$, where $\langle t(\lambda)\rangle$ is the photon mean time of flight, $v = c/n$ is the speed of light in vacuum, $n = 1.4$ is the tissue refractive index (assumed constant), and λ is the wavelength.

From μ_a at 686 and 830 nm by exploiting the Beer law,[44] HbO_2 and HHb were obtained assuming hemoglobin as the unique chromophore contributing to absorption. Hence, tHb and SO_2 were calculated. Unless differently specified, for each subject, the optical and hemodynamic parameters were averaged over all the 25 acquired DTOFs.

2.5 Statistical Analysis

The correlation (linear relationship) between two variables has been evaluated by computing the Pearson correlation coefficient r and the corresponding p-value. We considered no correlation for $|r| < 0.3$, low correlation $0.3 \leq |r| < 0.5$, moderate correlation for $0.5 \leq |r| < 0.7$, and high correlation for $0.7 \leq |r| < 1$.

3 Results

3.1 Demographic and Clinical Features of the Measured Subjects

A total of 307 healthy participants aged between 2 and 18 years were enrolled over 11 months. Two subjects initially enrolled were later excluded (not compliant due to intense crying during the measurements), resulting in 305 subjects. As shown in Table 1, the population is uniformly distributed according to gender and age, with 52% females (9.6 ± 4.6 years) and 48% males (9.5 ± 4.2 years).

Demographic and auxological descriptors are reported in Table 2. Data do not show abnormal trends. As expected, there is a strong correlation between age and head circumference (Pearson's correlation coefficient of 0.7 both for females and males) and a moderate correlation

Table 1 Enrolled subjects per age and gender.

Age (years)	Female (no.)	Male (no.)	Total (no.)	Female (%)	Male (%)	Total (%)
2 to 4	20	23	43	13	16	14
4 to 6	21	16	37	13	11	12
6 to 8	25	18	43	16	12	14
8 to 10	17	19	36	11	13	12
10 to 12	17	21	38	11	14	12
12 to 14	22	27	49	14	18	16
14 to 16	22	14	36	14	9	12
16 to 18	13	10	23	8	7	8
Total	157	148	305	100	100	100

Table 2 Auxological descriptors (average ± standard deviation) of the subjects per age and gender.

	BMI (kg/m^2)		BMI z-score		Head circumference (cm)	
Age (years)	Female	Male	Female	Male	Female	Male
2 to 4	15.0 ± 1.5	15.4 ± 1.5	−0.3 ± 1.0	−0.1 ± 1.2	48.9 ± 1.6	50.4 ± 1.5
4 to 6	14.8 ± 1.7	15.2 ± 1.8	−0.3 ± 1.0	−0.1 ± 1.3	50.8 ± 1.6	52.1 ± 1.3
6 to 8	16.7 ± 3.5	17.4 ± 6.0	0.7 ± 1.9	1.1 ± 3.6	52.2 ± 2.1	52.2 ± 1.8
8 to 10	19.6 ± 5.3	17.8 ± 3.5	1.5 ± 2.3	0.9 ± 1.9	52.8 ± 2.3	53.1 ± 1.4
10 to 12	19.6 ± 5.4	18.7 ± 3.3	0.9 ± 2.0	0.8 ± 1.5	53.5 ± 2.0	54.2 ± 1.8
12 to 14	22.6 ± 7.4	23.9 ± 7.1	1.4 ± 2.5	2.3 ± 2.8	54.7 ± 2.0	55.3 ± 1.8
14 to 16	22.4 ± 6.7	23.3 ± 4.8	0.6 ± 2.0	1.2 ± 1.5	54.9 ± 2.2	55.7 ± 2.9
16 to 18	23.1 ± 4.8	24.0 ± 6.4	0.6 ± 1.4	0.9 ± 2.0	55.9 ± 1.4	56.9 ± 2.8
Total	19.0 ± 5.9	19.3 ± 5.8	0.6 ± 1.9	0.9 ± 2.3	52.8 ± 2.9	53.5 ± 2.7

between age and BMI (Pearson's correlation coefficient of 0.5 and 0.6 for females and males, respectively).

3.2 Physiological Descriptors of the Measured Subjects

Table 3 shows the physiological descriptors (average ± standard deviation) of the subjects per age cluster and gender. Overall, no abnormal values for all parameters were recorded. The average HTC ranges from 34.3% to 41.9%. A moderate decrease of HR and BR with age is observed, as expected (Pearson's correlation coefficient for HR: $r = -0.6$ with p-value $= 1 \times 10^{-15}$ and $r = -0.5$ with p-value $= 2 \times 10^{-09}$, for females and males, respectively; Pearson's correlation coefficient for BR: $r = -0.4$ both for females and males with p-value $= 5 \times 10^{-08}$ and 1×10^{-07}, respectively). The average SpO_2 is higher than 98.1% with no correlation with age. As expected, HTC and Hb are strongly correlated (Pearson's correlation coefficient of 0.9 both for females and males with p-value $= 3 \times 10^{-71}$ and 4×10^{-60}, respectively), whereas a low correlation of both HTC and Hb with age is observed (Pearson's correlation coefficient for HTC: $r = 0.3$ with p-value $= 1 \times 10^{-04}$ and $r = 0.4$ with p-value $= 1 \times 10^{-08}$ for females and males, respectively; Pearson's correlation coefficient for Hb: $r = 0.3$ with p-value $= 1 \times 10^{-04}$ and $r = 0.4$ with p-value $= 5 \times 10^{-07}$ for females and males, respectively).

3.3 Optical Properties of the Measured Subjects

Table 4 reports the optical properties (average ± standard deviation) of the subjects at 686 and 830 nm per age (2-year clusters) and gender. For all variables, no differences can be found between the female and male groups at any age. The average μ_a values range from 0.16 to 0.25 cm^{-1} at 686 nm and from 0.17 to 0.24 cm^{-1} at 830 nm with an overall dispersion (as measured by the coefficient of variation over the entire population) of 21% at 686 nm and 18% at 830 nm. As expected, according to the empirical approximation of Mie's theory,[45] μ_s' is higher at 686 than at 830 nm with average values ranging from 13.2 to 14.4 cm^{-1} at 686 nm and from 11.3 to 12.3 cm^{-1} at 830 nm. Interestingly, the dispersion for scattering data is lower (almost half) than the dispersion for the absorption data with 10% at 686 nm and 9% at 830 nm. The average DPF varies from 4.2 to 5.2 at 686 nm and from 3.8 to 4.8 at 830 nm with 16% and 12% dispersion at 686 and 830 nm, respectively.

Figures 2 and 3 show the optical properties of the subjects (females and males at 686 and 830 nm, respectively) as a function of age, BMI z-score, and head circumference. Each dot represents a subject. As a general comment, we can notice the presence of few outliers in the distributions of the optical parameters. To evaluate the presence of correlations, we have reported in

Table 3 Physiological descriptors (average ± standard deviation) of the subjects per age and gender. HTC, hematocrit content (%); Hb, hemoglobin content (g/dl); HR, heart rate (beat/min); BR, breathing rate (breath/min); SpO_2, arterial oxygen saturation (%).

	HTC (%)		Hb (g/dl)		HR (beat/min)		BR (breath/min)		SpO_2 (%)	
Age (years)	Female	Male	Female	Male	Female	Male	Female	Male	Female	Male
2 to 4	34.3 ± 2.7	35.4 ± 3.5	11.6 ± 0.8	12.1 ± 1.2	112.0 ± 12.3	104.7 ± 15.7	25.8 ± 3.6	24.8 ± 3.2	98.8 ± 1.3	98.5 ± 1.3
4 to 6	34.3 ± 2.0	36.5 ± 3.7	11.8 ± 0.8	12.9 ± 1.3	103.4 ± 10.3	98.8 ± 14.0	23.0 ± 2.3	23.7 ± 3.4	98.7 ± 1.2	98.6 ± 0.8
6 to 8	36.4 ± 3.9	37.8 ± 4.3	12.3 ± 1.4	12.9 ± 1.7	88.4 ± 12.3	95.2 ± 16.9	23.0 ± 3.2	23.3 ± 4.2	98.5 ± 1.3	98.1 ± 1.0
8 to 10	36.1 ± 3.3	36.4 ± 2.3	12.5 ± 1.1	12.8 ± 1.0	93.6 ± 17.7	87.9 ± 10.6	24.2 ± 5.0	21.5 ± 2.7	98.8 ± 1.0	98.3 ± 1.3
10 to 12	38.5 ± 2.8	37.5 ± 3.4	13.3 ± 1.0	13.0 ± 1.3	85.9 ± 13.8	88.4 ± 8.7	21.8 ± 3.5	22.2 ± 2.9	98.4 ± 0.9	98.2 ± 0.9
12 to 14	38.5 ± 3.6	39.3 ± 3.1	13.2 ± 1.3	13.4 ± 1.2	83.4 ± 7.4	87.4 ± 15.0	20.0 ± 2.0	21.7 ± 3.7	99.0 ± 1.1	98.6 ± 1.0
14 to 16	37.3 ± 4.1	39.8 ± 2.6	12.6 ± 1.5	13.9 ± 0.7	78.6 ± 12.3	84.1 ± 15.6	20.2 ± 2.1	19.9 ± 2.3	99.2 ± 0.8	98.4 ± 1.3
16 to 18	36.4 ± 3.7	41.9 ± 3.2	12.5 ± 1.4	14.1 ± 0.9	83.5 ± 13.6	78.1 ± 9.5	20.8 ± 6.0	19.8 ± 2.4	98.5 ± 1.2	97.9 ± 0.7
Total	36.5 ± 3.7	37.8 ± 3.8	12.5 ± 1.3	13.0 ± 1.3	91.2 ± 16.5	91.6 ± 15.8	22.4 ± 4.0	22.3 ± 3.6	98.7 ± 1.1	98.4 ± 1.1

Table 4 Optical properties (average ± standard deviation) of the subjects at 686 and 830 nm per age and gender. Absorption coefficient, μ_a (cm^{-1}), reduced scattering coefficient μ_s' (cm^{-1}) DPF (–).

	μ_a (686 nm)		μ_a (830 nm)		μ_s' (686 nm)		μ_s' (830 nm)		DPF (686 nm)		DPF (830 nm)	
Age (years)	Female	Male	Female	Male	Female	Male	Female	Male	Female	Male	Female	Male
2 to 4	0.22 ± 0.03	0.24 ± 0.03	0.21 ± 0.02	0.23 ± 0.02	13.2 ± 1.4	14.0 ± 1.4	11.3 ± 1.2	11.9 ± 1.0	4.3 ± 1.3	4.2 ± 0.4	4.0 ± 0.4	3.9 ± 0.3
4 to 6	0.24 ± 0.03	0.25 ± 0.03	0.22 ± 0.03	0.24 ± 0.03	13.7 ± 1.0	14.0 ± 1.0	11.7 ± 0.7	12.1 ± 0.8	4.2 ± 0.4	4.2 ± 0.4	4.0 ± 0.3	3.9 ± 0.4
6 to 8	0.23 ± 0.04	0.24 ± 0.04	0.21 ± 0.03	0.23 ± 0.04	13.5 ± 1.3	13.7 ± 1.1	11.6 ± 1.0	11.9 ± 0.9	4.3 ± 0.3	4.2 ± 0.5	4.0 ± 0.4	4.0 ± 0.5
8 to 10	0.23 ± 0.03	0.22 ± 0.03	0.22 ± 0.03	0.21 ± 0.02	13.7 ± 0.9	13.5 ± 1.3	11.8 ± 0.8	11.7 ± 1.0	4.3 ± 0.4	4.3 ± 0.5	3.9 ± 0.3	4.0 ± 0.4
10 to 12	0.22 ± 0.06	0.22 ± 0.04	0.22 ± 0.05	0.22 ± 0.03	13.6 ± 1.1	14.0 ± 1.0	11.9 ± 0.8	12.0 ± 0.9	4.4 ± 0.6	4.6 ± 0.8	4.1 ± 0.7	4.0 ± 0.4
12 to 14	0.20 ± 0.04	0.23 ± 0.05	0.21 ± 0.04	0.24 ± 0.05	13.7 ± 1.2	14.2 ± 1.4	11.9 ± 0.9	12.3 ± 1.2	4.7 ± 0.6	4.5 ± 0.6	4.2 ± 0.4	4.0 ± 0.5
14 to 16	0.18 ± 0.03	0.23 ± 0.06	0.18 ± 0.03	0.25 ± 0.07	14.0 ± 1.4	14.4 ± 1.6	12.0 ± 1.2	12.2 ± 1.3	5.1 ± 0.7	4.6 ± 0.8	4.6 ± 0.6	3.8 ± 0.6
16 to 18	0.16 ± 0.04	0.20 ± 0.06	0.17 ± 0.03	0.21 ± 0.05	13.5 ± 1.0	13.9 ± 2.5	11.9 ± 0.8	11.8 ± 1.6	5.2 ± 0.6	4.9 ± 1.1	4.8 ± 0.4	4.1 ± 0.7
Total	0.21 ± 0.05	0.23 ± 0.05	0.21 ± 0.04	0.23 ± 0.04	13.6 ± 1.2	14.0 ± 1.4	11.7 ± 1.0	12.0 ± 1.1	4.6 ± 0.8	4.4 ± 0.7	4.2 ± 0.5	4.0 ± 0.5

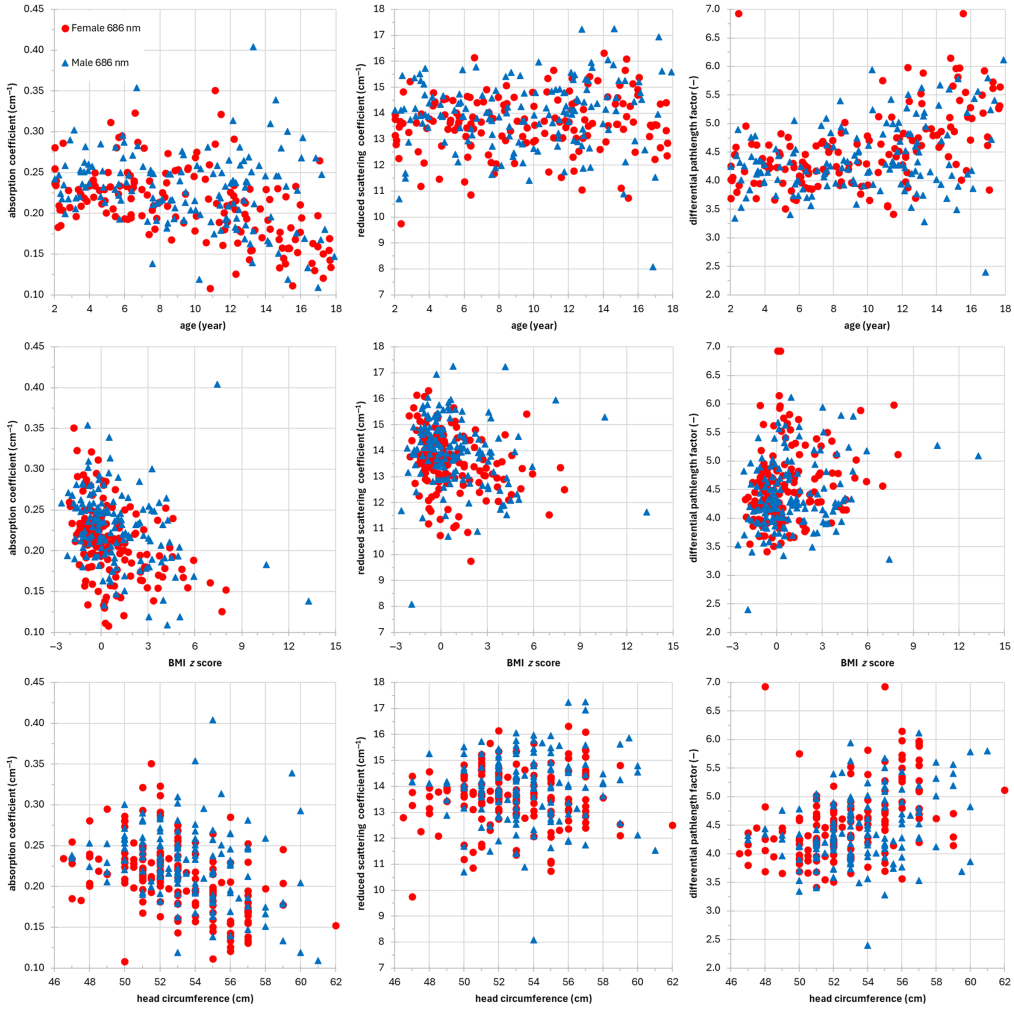

Fig. 2 Optical properties of the subjects (female, red circles; male, blue triangles) at 686 nm as a function of age (left column), BMI z-score (middle column), and head circumference (right column). Top row: absorption coefficient (cm^{-1}), middle row: reduced scattering coefficient (cm^{-1}), and bottom row: differential pathlength factor.

Table 5 the Pearson's correlation coefficient r and the related p-value. We have a moderate/low inverse correlation with age for μ_a in females ($r = -0.5$ and -0.3 with p-value $= 4 \times 10^{-11}$ and 2×10^{-05} at 686 and 830 nm, respectively) and no correlation in males. No correlation with age is found for μ_s' for both females and males. There is a moderate/low correlation ($r = 0.5$ and 0.4 with p-value $= 8 \times 10^{-12}$ and 4×10^{-09} at 686 and 830 nm, respectively) with age for DPF in females, whereas there is a low correlation only at 686 nm ($r = 0.3$ with p-value $= 9 \times 10^{-05}$) for DPF in males. Regarding the correlation with BMI z-score, we have a low inverse correlation for μ_a in females ($r = -0.4$ and -0.3 with p-value $= 1 \times 10^{-07}$ and 2×10^{-05} at 686 and 830 nm, respectively) and a low correlation in males only at 686 nm ($r = -0.3$ with p-value $= 2 \times 10^{-04}$). No correlation with BMI z-score for μ_s' is observed in males, whereas a low correlation at 686 nm is found in females ($r = -0.3$ with p-value $= 4 \times 10^{-04}$). Finally, no correlation with BMI z-score for DPF is found in the female and male groups. A moderate or low inverse correlation ($r = -0.5$ and -0.3 with p-value $= 3 \times 10^{-09}$ and 6×10^{-05} at 686 nm and 830 nm, respectively) with head circumference is observed for μ_a in females, whereas we have a low inverse correlation only at 686 nm ($r = -0.3$ with p-value $= 6 \times 10^{-04}$) in males. Again, no correlation is found for μ_s' in both the female and male groups. A low correlation with head circumference for DPF in females ($r = 0.4$ both at 686 and

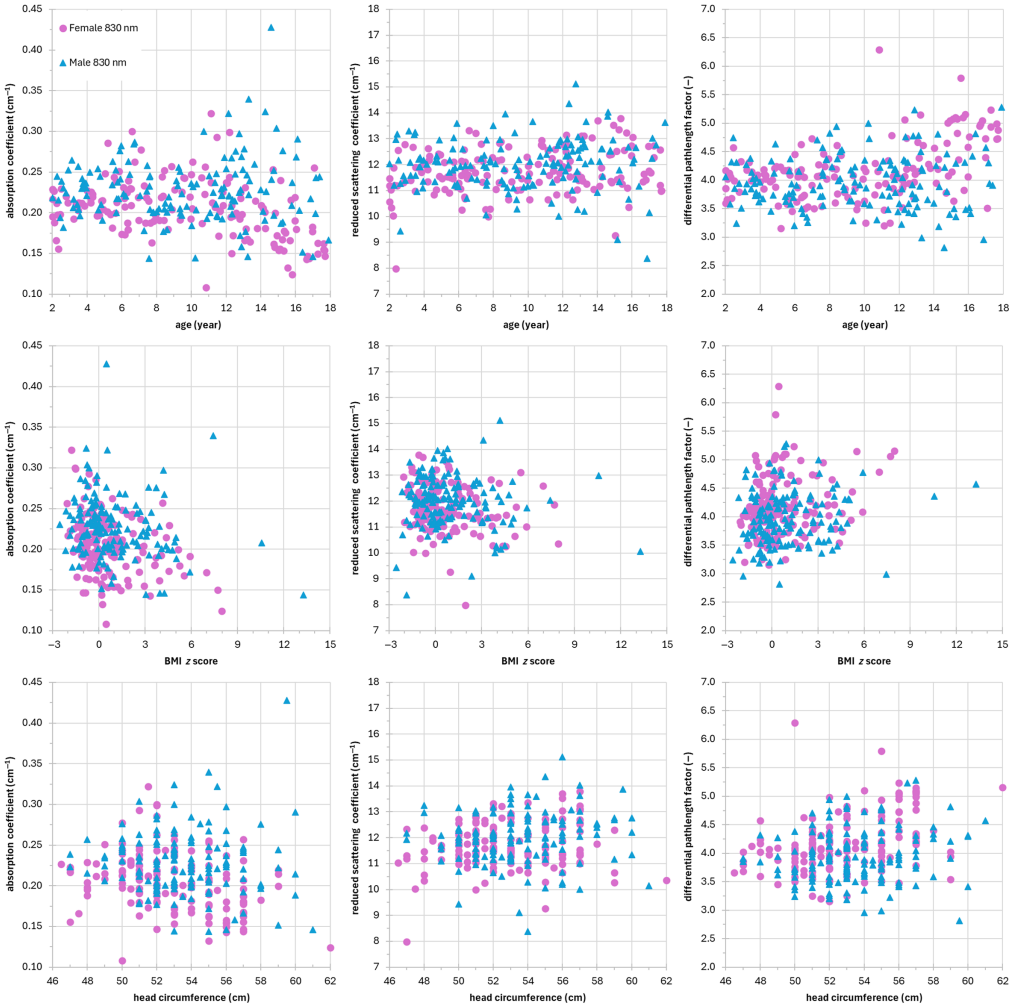

Fig. 3 Optical properties of the subjects (female, purple squares; male, cyan diamonds) at 830 nm as a function of age (left column), BMI *z*-score (middle column), and head circumference (right column). Top row: absorption coefficient (cm^{-1}), middle row: reduced scattering coefficient (cm^{-1}), and bottom row: differential pathlength factor.

830 nm with $p-\text{value} = 1 \times 10^{-8}$ and 1×10^{-06}, respectively) and a low correlation in males at 686 nm ($r = 0.3$ with $p\text{-value} = 2 \times 10^{-5}$) are observed.

We have compared the results for the DPF (with no distinction between females and males) with the general equation $\text{DPF}(A, \lambda) = \alpha + \beta A^{\gamma} + \delta\lambda^3 + \varepsilon\lambda^3 + \zeta\lambda$, where A is the age in years and λ the wavelength in nanometers, derived by Scholkmann and Wolf.[46] When using the original values for parameters $\alpha - \zeta$, the agreement is not perfect as shown in Fig. 4(a). However, we notice that with only a slight change (<0.5%) from $\alpha = 223.3$ to $\alpha = 222.2$ (obtained by minimizing the error between the DPF model and data), the agreement improves as shown in Fig. 4(b). However, the correlation is low or null because the Pearson correlation coefficient is 0.3 and 0.2, respectively at 686 nm at 830 nm, probably affected by some outliers.

3.4 Hemodynamic Properties of the Measured Subjects

Table 6 shows the hemodynamic parameters (average ± standard deviation) of the subjects per age cluster and gender. For all variables, no differences can be found between the female and male groups at any age. The average HbO_2 and HHb values range from 55.9 to 86.0 μM and from 25.4 to 39.3 μM, respectively, with an overall dispersion of 18% and 23%. These values result in an average tHb ranging from 81.3 to 120.0 μM with 18% dispersion and average SO_2 in the range from 64.3% to 71.8% with 6% dispersion.

Table 5 Pearson's correlation coefficient r and corresponding p-value for optical properties (bold $0.5 \leq |r| < 0.7$ moderate correlation, italics $0.3 \leq |r| < 0.5$ low correlation, no emphasis $0 \leq |r| < 0.3$ no correlation, and bold italics p-value ≥ 0.05).

		μ_a (686 nm)		μ_a (830 nm)		μ_s' (686 nm)		μ_s' (830 nm)		DPF (686 nm)		DPF (830 nm)	
		Female	Male	Female	Male	Female	Male	Female	Male	Female	Male	Female	Male
Age	r	**−0.5**	−0.2	*−0.3*	0.0	0.1	0.1	0.2	0.1	**0.5**	*0.3*	*0.4*	0.0
	p-value	4×10^{-11}	5×10^{-03}	2×10^{-05}	***7 × 10⁻⁰¹***	***2 × 10⁻⁰¹***	***4 × 10⁻⁰¹***	***5 × 10⁻⁰³***	***5 × 10⁻⁰¹***	8×10^{-12}	9×10^{-05}	4×10^{-09}	***7 × 10⁻⁰¹***
BMI z-score	r	*−0.4*	*−0.3*	*−0.3*	−0.2	*−0.3*	−0.2	−0.2	−0.1	0.2	0.2	0.2	0.1
	p-value	1×10^{-07}	2×10^{-04}	2×10^{-05}	2×10^{-02}	4×10^{-04}	4×10^{-02}	1×10^{-02}	***2 × 10⁻⁰¹***	2×10^{-03}	5×10^{-03}	7×10^{-03}	***9 × 10⁻⁰²***
Head circ.	r	**−0.5**	*−0.3*	*−0.3*	0.0	0.1	0.0	0.2	0.1	*0.4*	*0.3*	*0.4*	0.1
	p-value	3×10^{-09}	6×10^{-04}	6×10^{-05}	***8 × 10⁻⁰¹***	***4 × 10⁻⁰¹***	***6 × 10⁻⁰¹***	***6 × 10⁻⁰²***	***2 × 10⁻⁰¹***	1×10^{-08}	2×10^{-05}	1×10^{-06}	***1 × 10⁻⁰¹***

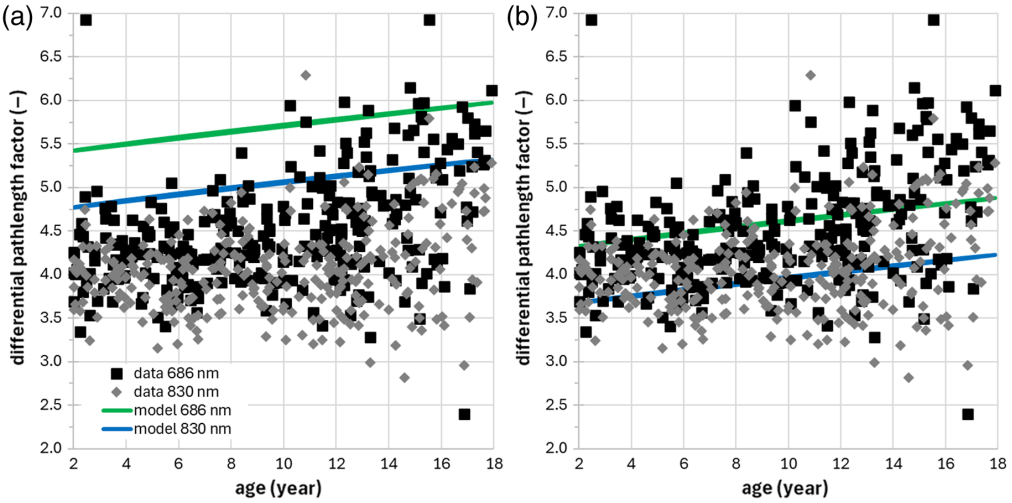

Fig. 4 DPF at 686 and 830 nm as a function of age and estimates obtained by the general equation[47] with $\alpha = 223.3$ (a) and with $\alpha = 222.2$ (b).

Table 6 Hemodynamic properties (average ± standard deviation) of the subjects per age and gender.

Age (years)	HbO_2 (μM)		HHb (μM)		tHb (μM)		SO_2 (%)	
	Female	Male	Female	Male	Female	Male	Female	Male
2 to 4	65.9 ± 8.2	72.6 ± 8.0	36.3 ± 5.5	39.3 ± 5.0	102.2 ± 10.9	111.8 ± 10.9	64.5 ± 3.9	64.9 ± 3.1
4 to 6	69.4 ± 8.7	77.3 ± 9.7	38.5 ± 6.0	39.2 ± 5.4	107.9 ± 13.3	116.6 ± 13.5	64.3 ± 2.8	66.3 ± 2.8
6 to 8	69.5 ± 11.8	74.4 ± 12.2	36.4 ± 6.3	37.5 ± 7.9	105.9 ± 16.8	112.0 ± 17.9	65.5 ± 3.1	66.6 ± 3.6
8 to 10	72.3 ± 8.5	70.4 ± 8.7	36.5 ± 5.7	35.1 ± 5.5	108.8 ± 12.9	105.4 ± 11.0	66.5 ± 3.0	66.7 ± 4.3
10 to 12	74.0 ± 14.3	73.9 ± 12.1	34.7 ± 10.4	33.8 ± 7.0	108.8 ± 23.9	107.7 ± 16.3	68.5 ± 3.4	68.7 ± 4.5
12 to 14	70.1 ± 12.0	80.1 ± 15.4	30.2 ± 6.2	35.7 ± 9.3	100.3 ± 17.2	115.8 ± 22.7	70.0 ± 3.1	69.3 ± 3.9
14 to 16	61.7 ± 11.6	86.0 ± 24.1	27.5 ± 5.8	34.0 ± 10.8	89.2 ± 16.0	120.0 ± 31.7	69.2 ± 3.9	71.8 ± 6.0
16 to 18	55.9 ± 9.4	73.5 ± 15.6	25.4 ± 6.5	30.2 ± 11.2	81.3 ± 15.0	103.7 ± 24.1	69.0 ± 3.6	71.5 ± 5.9
Total	67.7 ± 11.9	75.9 ± 14.2	33.5 ± 7.9	36.0 ± 8.2	101.2 ± 18.3	111.9 ± 19.5	67.1 ± 4.0	67.9 ± 4.8

Figure 5 shows the hemodynamic parameters of the subjects (female and male) as a function of age, BMI z-score, or head circumference, whereas in Table 7, we report the corresponding Pearson's correlation coefficients r and p-values. No correlation with age for HbO_2 is found for both females and males. Conversely, moderate ($r = -0.5$ with p-value $= 1 \times 10^{-12}$) inverse correlation with age is found for HHb in females and low inverse correlation ($r = -0.3$ with p-value $= 3 \times 10^{-04}$) in males. Low ($r = -0.4$ with p-value $= 3 \times 10^{-06}$) inverse correlation with age is present for tHb in females only, whereas a moderate correlation for SO_2 is found for both females and males ($r = 0.5$ with p-value $= 1 \times 10^{-12}$ and 3×10^{-09}, respectively).

Low inverse correlation with BMI z-score is found for HbO_2 in females ($r = -0.4$ with p-value $= 4 \times 10^{-06}$), whereas no correlation is observed in males. A moderate inverse correlation ($r = -0.6$ with p-value $= 4 \times 10^{-15}$) for HHb is observed in females, and a low inverse correlation ($r = -0.4$ with p-value $= 8 \times 10^{-06}$) in males. There is a moderate inverse correlation ($r = -0.5$ with p-value $= 1 \times 10^{-10}$) with BMI z-score for tHb in females but no correlation

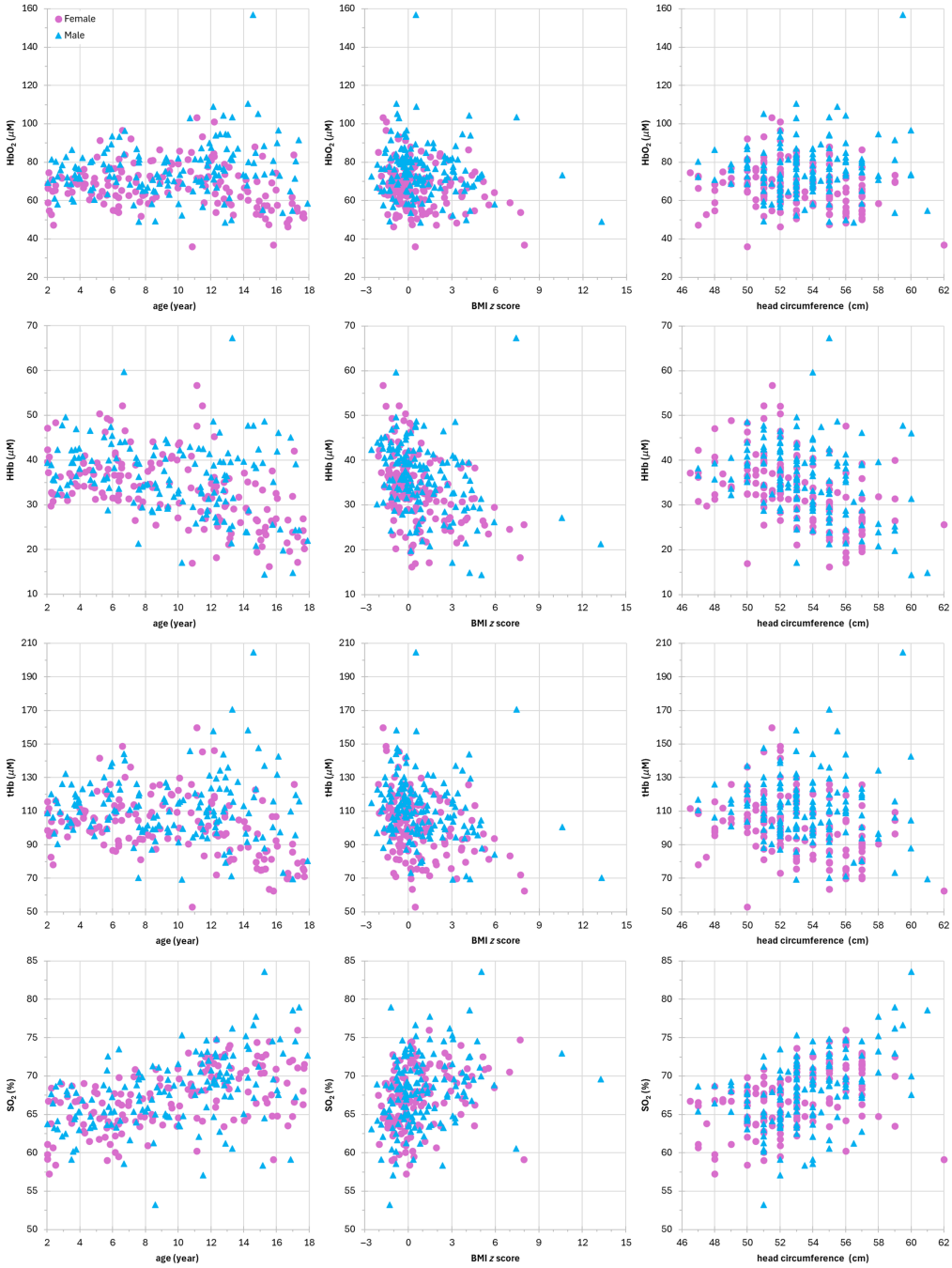

Fig. 5 Hemodynamic parameters of the subjects (female, purple circle; male, cyan triangle) as a function of age (left column), BMI *z*-score (middle column), and head circumference (right column). Rows from top to bottom: HbO_2 (μM), HHb (μM), tHb (μM), and SO_2 (%).

in males. SO_2 has a low correlation with BMI *z*-score for both females and males ($r = 0.4$ for both groups with p-value $= 5 \times 10^{-08}$ and 1×10^{-07}, respectively).

No correlation with head circumference for HbO_2 is observed for both females and males. Moderate inverse correlation ($r = -0.5$ with p-value $= 4 \times 10^{-10}$) is found for HHb in females and low inverse correlation ($r = -0.3$ with p-value $= 3 \times 10^{-05}$) in males. There is a low correlation ($r = 0.3$ with p-value $= 1 \times 10^{-05}$) for tHb in females but no correlation in males. There is a low correlation ($r = 0.4$ with p-value $= 4 \times 10^{-09}$) for SO_2 in females and moderate correlation ($r = 0.5$ with p-value $= 1 \times 10^{-09}$) in males.

Table 7 Pearson's correlation coefficient r and corresponding p-value for hemodynamic properties (bold $0.5 \leq |r| < 0.7$ moderate correlation, italics $0.3 \leq |r| < 0.5$ low correlation, no emphasis $0 \leq |r| < 0.3$ no correlation, and bold italics p-value ≥ 0.05.

		HbO_2 (μM)		HHb (μM)		tHb (μM)		SO_2 (%)	
		Female	Male	Female	Male	Female	Male	Female	Male
Age	r	−0.2	0.2	**−0.5**	*−0.3*	*−0.4*	0.0	**0.5**	**0.5**
	p-value	9×10^{-03}	***5 × 10⁻⁰²***	1×10^{-12}	3×10^{-04}	3×10^{-06}	***9 × 10⁻⁰¹***	1×10^{-12}	3×10^{-09}
BMI z-score	r	*−0.4*	0.0	**−0.6**	*−0.4*	**−0.5**	−0.2	*0.4*	*0.4*
	p-value	4×10^{-06}	***7 × 10⁻⁰¹***	4×10^{-15}	8×10^{-06}	1×10^{-10}	4×10^{-02}	5×10^{-08}	1×10^{-07}
Head circ.	r	−0.2	0.1	**−0.5**	*−0.3*	*−0.3*	−0.1	*0.4*	**0.5**
	p-value	9×10^{-03}	***2 × 10⁻⁰¹***	4×10^{-10}	3×10^{-05}	1×10^{-05}	***5 × 10⁻⁰¹***	4×10^{-09}	1×10^{-09}

3.5 Precision of the Estimates of Optical and Hemodynamic Parameters of the Measured Subjects

The precision of measured optical and hemodynamic properties was evaluated by calculating for each subject the coefficient of variation $\mathrm{CV}(x) = 100\sigma(x)/m(x)$, where x is the variable under study (e.g., μ_s' or HbO_2), $m(x)$ is the average, and $\sigma(x)$ is the standard deviation of the five

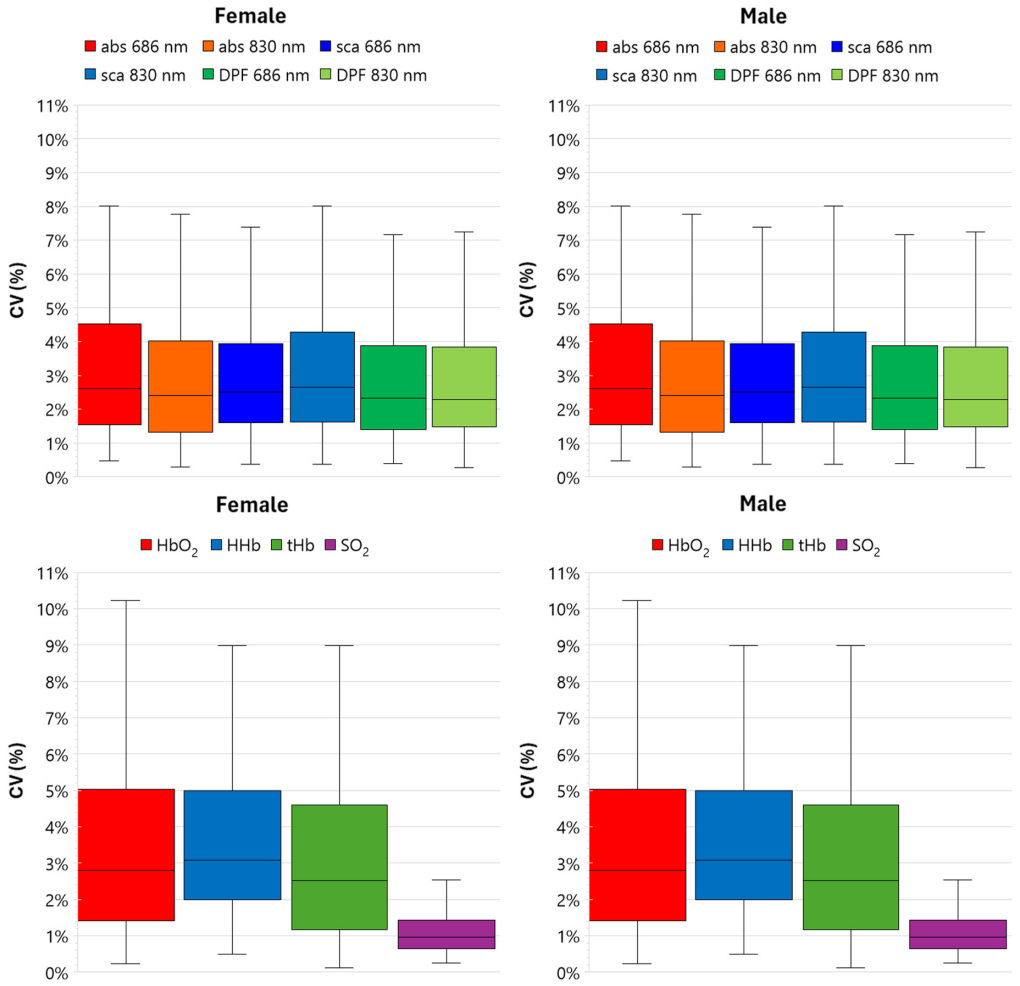

Fig. 6 CV over five repositionings for optical parameters (top row) and hemodynamic parameters (bottom row). Left column: female; right column: male.

repositionings. Figure 6 shows the boxplots of the CV for optical properties and hemodynamic parameters for all the subjects. The interquartile (25% to 75%) CV for the optical properties is in the range 1% to 5%. The same holds for HbO_2, HHb, and tHb, whereas noticeably, SO_2 show a dispersion <2%.

4 Discussion

TD NIRS measurements on a large cohort of pediatric patients were performed in a hospital. Absolute values for baseline optical (absorption coefficient, reduced scattering coefficient, and differential pathlength factor at 686 and 830 nm) and hemodynamic parameters (oxygenated and deoxygenated hemoglobin content, total hemoglobin content, and cerebral oxygen saturation) were shown as a function of age and of demographic variables. The TD NIRS device was operated by the clinicians. Each operator attended a short (10 min) training course to learn the basic functions of the device. No adverse effects on the subjects or malfunctioning of the device were recorded during the measurement campaign.

Subject admission to the hospital was related to different causes, such as endocrinological, neurological, osteoarticular, gastroenterological, infectious, or respiratory. According to the inclusion criteria, subjects were measured just before discharge from the hospital, when clinical parameters were stable, and no treatment was ongoing. Therefore, we reasonably hypothesize no effect of the admission cause on the TD NIRS results. Moreover, at the time of measurements, all subjects were calm and cooperative with normal parameters.

Data reproducibility (i.e., dispersion of values during repositioning in each subject) was good being <5% for most of the measured variables and <2% for SO_2. Precision after probe replacement is indicated as the first problem in cerebral oximetry by NIRS.[48] In laboratory settings, the NIRSBOX device demonstrated excellent precision (<1%) after probe replacement on tissue phantoms for both μ_a and μ_s', whereas slightly higher values (<3% for optical properties and hemodynamic parameters) were found for *in vivo* measurements of the human muscle.[49] Then, the dispersion of the hemodynamic values during repositioning reported in this study is consistent with laboratory tests and also with other recently developed CW NIRS cerebral oximeters tested on neonates.[20,50] Based on our previous experience with TD NIRS, we expect that similar precision values could be obtained with the TD NIRS device also in neonates and adults.

In analyzing the correlation between optical parameters and anthropometric measurements (BMI z-score, age, and head circumference), several key observations emerge. A general trend of higher absorption values in males compared with females was noted. In addition, this difference appears to increase with age. DPF values demonstrated low to moderate correlations with age and head circumference in both sexes but showed no correlation with BMI z-score. This lack of correlation is likely due to the fact that BMI z-score is already adjusted for age and sex, indicating that cerebral DPF values may be linked to growth indicators such as age and head circumference but not to BMI variations.

These anthropometric differences partially extend to cerebral tissue oximetry parameters. A low to moderate correlation was observed between SO_2 and BMI z-score, age, and head circumference. Interestingly, tHb was correlated with these anthropometric variables only in females, driven primarily by HHb levels. This suggests that auxological factors, particularly in females, may influence cerebral oxygenation metrics. These findings highlight the importance of considering both growth-related variables and BMI when interpreting reference cerebral oximetry values in pediatric populations. Specifically, older and heavier children tend to exhibit slightly higher cerebral SO_2 values, whereas younger and lighter children, particularly females, show lower brain tHb content.

Overall, the measured optical and hemodynamic properties show values coherent with the literature data.[33–36] These data can be helpful for improving the accuracy of other techniques such as DCS and SCOS that rely on values of the optical parameters to derive estimates of tissue perfusion.[51] Indeed, the accuracy of the measured quantities strongly depends on the physical model used for data analysis. We (such as the majority of the published papers) have used a simple homogeneous model; therefore, values refer to the average properties of the tissue beneath the probe. We have shown in a previous study on adults[27] that the use of a TD NIRS device with a

homogeneous model can provide values of the absorption coefficient closer to the estimates obtained by a two-layer model for the deep layer than to the estimates for the superficial layer. Moreover, penetration depth in TD NIRS is independent from the source–detector distance, whereas it relates to the photon time-of-flight.[52] From TD NIRS simulations in a two-layer diffusive medium,[53] we have recently shown that the influence on the penetration depth of the thickness of the superficial layer can be reduced by including photons with late arrival time at the detector, such as it is normally done when fitting TD NIRS data with the photon diffusion model.[54] For the above observations, we think that the use of the same source–detector distance for all subjects has minimal influence on the results, despite the different anatomical sizes of the head. Therefore, as human cranial vault thickness in the pediatric population is significantly lower than in adults,[55] we are confident that the values for hemodynamic parameters (being derived from the absorption coefficient) are more representative of the cortical tissue than the extracerebral tissue. Nonetheless, more accurate modeling (e.g., with numerical Monte Carlo simulations based on 3D anatomical mesh) would provide more robust estimates.[32,56]

The dispersion over the full cohort of the optical properties (∼20% for μ_a, 10% for μ_s', and 14% for DPF) and of the hemodynamic parameters (∼20% for HbO_2, HHb, and tHb) is higher than the dispersion in physiological parameters (∼10% for HTC and Hb), being probably affected by the dispersion in BMI (∼30%). This suggests that individual measurements of optical coefficients and hemodynamic contents should be preferred to the average data taken from the literature. Interestingly, SO_2 shows an overall reduced dispersion of ∼6% and that is supportive being this the most relevant clinical parameter.

In the derivation of the hemodynamic parameters from the absorption coefficient, we have only considered the contribution of hemoglobin, neglecting contributions from other chromophores such as water and lipids. In general, the water content of normal tissues is typically <80% (except for gray matter, placenta, and fetus).[57] In the extreme case that water contributes 90% to tissue absorption, the errors in the estimate of hemodynamic parameters are 3%, −21%, −13%, and −9% for HHb, HbO_2, tHb, and SO_2, respectively. Water absorption is in fact larger at 830 nm than at 686 nm; therefore, it will mainly affect the estimate of HbO_2. Lipid absorption at short near-infrared wavelengths is low;[47] therefore, even 90% of lipids contribute minimally to light absorption at 686 and 830 nm. In this case, in fact, the errors in the estimate of hemodynamic parameters are −1%, −5%, −4%, and −1% for HHb, HbO_2, tHb, and SO_2, respectively.

5 Conclusion

This study provided baseline values for optical and hemodynamic parameters in a large cohort of healthy pediatric subjects with good precision, providing a foundation for future investigations into clinically relevant deviations in these parameters. Although we have observed some correlations of optical and hemodynamic properties with auxological parameters, we do believe that more data are needed to draw robust inferences.

Disclosures

D. Contini and A. Torricelli are co-founders of PIONIRS S.r.l., a spin-off company of the Politecnico di Milano.

Code and Data Availability

The codes and datasets generated during and analyzed during the current study are available from the corresponding author upon reasonable request.

Acknowledgments

Horizon 2020 Framework Programme of the European Union (PLS; Grant Agreement No. 863087)—European Innovation Council under the Pathfinder Open call (Prometeus; Grant Agreement No. 101099093).

References

1. H. Ayaz et al., "Optical imaging and spectroscopy for the study of the human brain: status report," *Neurophotonics* **9**(Suppl. 2), S24001 (2022).
2. M. L. Hansen et al., "Cerebral near-infrared spectroscopy monitoring (NIRS) in children and adults: a systematic review with meta-analysis," *Pediatr. Res.* **96**, 856–867 (2022).
3. A. la Cour, G. Greisen, and S. Hyttel-Sorensen, "*In vivo* validation of cerebral near-infrared spectroscopy: a review," *Neurophotonics* **5**(4), 040901 (2018).
4. M. Ferrari and V. Quaresima, "A brief review on the history of human functional near-infrared spectroscopy (fNIRS) development and fields of application," *Neuroimage* **63**(2) 921–935 (2012).
5. F. Scholkmann et al., "A review on continuous wave functional near-infrared spectroscopy and imaging instrumentation and methodology," *Neuroimage* **85 Pt 1**, 6–27 (2014).
6. A. von Lühmann et al., "Towards Neuroscience of the Everyday World (NEW) using functional near-infrared spectroscopy," *Curr. Opin. Biomed. Eng.* **18**, 100272 (2021).
7. W. Zhou, M. Zhao, and V. J. Srinivasan, "Interferometric diffuse optics: recent advances and future outlook," *Neurophotonics* **10**(1), 013502 (2023).
8. M. A. Yücel et al., "Best practices for fNIRS publications [published correction appears in neurophotonics," **8**(1), 019802 (2021).
9. https://openfnirs.org/ [last accessed 2024 May 18].
10. F. Martelli et al., "Light propagation through biological tissue and other diffusive media: theory, solutions, and validations," 2nd Ed., SPIE Book, p. 698 (2022).
11. Q. Fang and S. Yan, "MCX Cloud—a modern, scalable, high-performance and in-browser Monte Carlo simulation platform with cloud computing," *J. Biomed. Opt.* **27**(8), 083008 (2022).
12. S. Ijichi et al., "Developmental changes of optical properties in neonates determined by near-infrared time-resolved spectroscopy," *Pediatr. Res.* **58**(3), 568–573 (2005).
13. S. J. Arri et al., "Precision of cerebral oxygenation and hemoglobin concentration measurements in neonates measured by near-infrared spectroscopy," *J. Biomed. Opt.* **16**(4), 047005 (2011).
14. J. W. Barker, A. Panigrahy, and T. J. Huppert, "Accuracy of oxygen saturation and total hemoglobin estimates in the neonatal brain using the semi-infinite slab model for FD-NIRS data analysis," *Biomed. Opt. Express.* **5**(12), 4300–4312 (2014).
15. N. Roche-Labarbe et al., "Somatosensory evoked changes in cerebral oxygen consumption measured non-invasively in premature neonates," *Neuroimage* **85 Pt 1**(0 1), 279–286 (2014).
16. P. Y. Lin et al., "Reduced cerebral blood flow and oxygen metabolism in extremely preterm neonates with low-grade germinal matrix-intraventricular hemorrhage," *Sci. Rep.* **6**, 25903 (2016).
17. L. Spinelli et al., "*In vivo* measure of neonate brain optical properties and hemodynamic parameters by time-domain near-infrared spectroscopy," *Neurophotonics* **4**(4), 041414 (2017).
18. S. Nakamura et al., "Simultaneous measurement of cerebral hemoglobin oxygen saturation and blood volume in asphyxiated neonates by near-infrared time-resolved spectroscopy," *Brain Dev.* **37** (10), 925–932 (2015).
19. Z. Kovacsova et al., "Absolute quantification of cerebral tissue oxygen saturation with multidistance broadband NIRS in newborn brain," *Biomed. Opt. Express.* **12**(2), 907–925 (2021).
20. A. Avian et al., "Precision of time-resolved near-infrared spectroscopy-based measurements of cerebral oxygenation in preterm infants," *Neurophotonics* **8**(4), 045001 (2021).
21. A. Liebert et al., "Time-resolved multidistance near-infrared spectroscopy of the adult head: intracerebral and extracerebral absorption changes from moments of distribution of times of flight of photons," *Appl. Opt.* **43**(15), 3037–3047 (2004).
22. J. Choi et al., "Noninvasive determination of the optical properties of adult brain: near-infrared spectroscopy approach," *J. Biomed. Opt.* **9**(1), 221–229 (2004).
23. V. Quaresima et al., "Bilateral prefrontal cortex oxygenation responses to a verbal fluency task: a multichannel time-resolved near-infrared topography study," *J. Biomed. Opt.* **10**(1), 11012 (2005).
24. T. S. Leung et al., "Measurement of the absolute optical properties and cerebral blood volume of the adult human head with hybrid differential and spatially resolved spectroscopy," *Phys. Med. Biol.* **51**(3), 703–717 (2006).
25. L. Gagnon et al., "Double-layer estimation of intra- and extracerebral hemoglobin concentration with a time-resolved system," *J. Biomed. Opt.* **13**(5), 054019 (2008).
26. B. Hallacoglu et al., "Absolute measurement of cerebral optical coefficients, hemoglobin concentration and oxygen saturation in old and young adults with near-infrared spectroscopy," *J. Biomed. Opt.* **17**(8), 081406 (2012).
27. A. Farina et al., "*In-vivo* multilaboratory investigation of the optical properties of the human head," *Biomed. Opt. Express.* **6**(7), 2609–2623 (2015).
28. H. Auger et al., "Quantification of extra-cerebral and cerebral hemoglobin concentrations during physical exercise using time-domain near infrared spectroscopy," *Biomed. Opt. Express.* **7**(10), 3826–3842 (2016).

29. G. Giacalone et al., "Cerebral time domain-NIRS: reproducibility analysis, optical properties, hemoglobin species and tissue oxygen saturation in a cohort of adult subjects," *Biomed. Opt. Express.* **8**(11), 4987–5000 (2017).
30. F. Scholkmann et al., "Absolute values of optical properties (μ_a, μ_s', μ_{eff} and DPF) of human head tissue: dependence on head region and individual," *Adv. Exp. Med. Biol.* **1072**, 325–330 (2018).
31. S. Fantini and A. Sassaroli, "Frequency-domain techniques for cerebral and functional near-infrared spectroscopy," *Front. Neurosci.* **14**, 300 (2020).
32. T. C. Kao and K. B. Sung, "Quantifying tissue optical properties of human heads *in vivo* using continuous-wave near-infrared spectroscopy and subject-specific three-dimensional Monte Carlo models," *J. Biomed. Opt.* **27**(8), 083021 (2022).
33. H. M. Watzman et al., "Arterial and venous contributions to near-infrared cerebral oximetry," *Anesthesiology* **93**(4), 947–953 (2000).
34. M. Dehaes et al., "Assessment of the frequency-domain multi-distance method to evaluate the brain optical properties: Monte Carlo simulations from neonate to adult," *Biomed. Opt. Express.* **2**(3), 552–567 (2011).
35. F. Tian et al., "Regional cerebral abnormalities measured by frequency-domain near-infrared spectroscopy in pediatric patients during extracorporeal membrane oxygenation," *ASAIO J.* **63**(5), e52–e59 (2017).
36. T. Suemori et al., "Clinical significance of assessing cerebral blood volume by time-domain near-infrared spectroscopy in children with congenital heart disease," *Paediatr. Anaesth.* **32**(3), 413–420 (2022).
37. J. A. DiNardo, "Cerebral oximetry in children: so NIRS yet so far," *Anesth Analg.* **128**(4), 605–606 (2019).
38. M. Lacerenza et al., "Performance and reproducibility assessment across multiple time-domain near-infrared spectroscopy device replicas," *Proc. SPIE* **11951**, 1195108 (2022).
39. https://www.pionirs.com/probes/ [last accessed 2024 May 18].
40. WHO Multicentre Growth Reference Study Group, "WHO Child Growth Standards based on length/height, weight and age," *Acta. Paediatr.* **450**, 76–85 (2006).
41. https://www.who.int/toolkits/child-growth-standards/standards/body-mass-index-for-age-bmi-for-age [last accessed 2024 May 18].
42. https://www.who.int/tools/growth-reference-data-for-5to19-years/indicators/bmi-for-age [last accessed 2024 May 18].
43. D. Contini, F. Martelli, and G. Zaccanti, "Photon migration through a turbid slab described by a model based on diffusion approximation. I. Theory," *Appl. Opt.* **36**(19), 4587–4599 (1997).
44. https://omlc.org/spectra/hemoglobin/ [last accessed 2024 May 18].
45. J. R Mourant et al., "Predictions and measurements of scattering and absorption over broad wavelength ranges in tissue phantoms," *Appl. Opt.* **36**(4), 949–957 (1997).
46. F. Scholkmann and M. Wolf, "General equation for the differential pathlength factor of the frontal human head depending on wavelength and age," *J. Biomed. Opt.* **18**(10), 105004 (2013).
47. R. L. van Veen et al., "Determination of visible near-IR absorption coefficients of mammalian fat using time- and spatially resolved diffuse reflectance and transmission spectroscopy," *J. Biomed. Opt.* **10**(5), 054004 (2005).
48. G. Greisen et al., "Cerebral oximetry in preterm infants: an agenda for research with a clear clinical goal," *Neurophotonics* **3**(3), 031407 (2016).
49. M. Lacerenza et al., "Wearable and wireless time-domain near-infrared spectroscopy system for brain and muscle hemodynamic monitoring," *Biomed. Opt. Express* **11**(10), 5934–5949 (2020).
50. S. Kleiser et al., "*In vivo* precision assessment of a near-infrared spectroscopy-based tissue oximeter (OxyPrem v1.3) in neonates considering systemic hemodynamic fluctuations," *J. Biomed. Opt.* **23**(6), 067003 (2018).
51. T. Durduran et al., "Diffuse optics for tissue monitoring and tomography," *Rep. Prog. Phys.* **73**(7), 076701 (2010).
52. F. Martelli et al., "There's plenty of light at the bottom: statistics of photon penetration depth in random media," *Sci. Rep.* **6**, 27057 (2016).
53. F. Martelli et al., "Statistics of maximum photon penetration depth in a two-layer diffusive medium," *Biomed. Opt. Express.* **15**(2), 1163–1180 (2024).
54. F. Martelli et al., "Optimal estimation reconstruction of the optical properties of a two-layered tissue phantom from time-resolved single-distance measurements," *J. Biomed. Opt.* **20**(11), 115001 (2015).
55. H. H. De Boer, A. E. Van der Merwe, and V. V. Soerdjbalie-Maikoe, "Human cranial vault thickness in a contemporary sample of 1097 autopsy cases: relation to body weight, stature, age, sex and ancestry," *Int. J. Legal Med.* **130**(5), 1371–1377 (2016).
56. C. Amendola et al., "Accuracy of homogeneous models for photon diffusion in estimating neonatal cerebral hemodynamics by TD-NIRS," *Biomed. Opt. Express.* **12**(4), 1905–1921 (2021).
57. I. C. Kiricuta, Jr and V. Simplăceanu, "Tissue water content and nuclear magnetic resonance in normal and tumor tissues," *Cancer Res.* **35**(5), 1164–1167 (1975).

Valeria Calcaterra is a pediatric researcher at the University of Pavia and a pediatrician at the Department of Pediatrics, Vittore Buzzi Children's Hospital, Milan, Italy. She is the author of more than 350 papers in international peer-reviewed journals. She participated in over 30 national and international projects. The main fields of her research have been pediatric endocrinological diseases, diabetology, childhood obesity, cardio-metabolic complications related to obesity, malnutrition in pediatric disability, preventive and translational medicine, telemedicine, and health systems.

Michele Lacerenza is the chief technical officer at PIONIRS s.r.l. He received his MSc degree in physics engineering, nano-optics, and photonics from Politecnico di Milano where he pursued his PhD in physics (2022). His focus involves the development and exploitation of compact photonic platforms for cerebral and muscle hemodynamics. He served as a reviewer, director, and chair/organizer of international scientific events and participated in high-impact international research projects. Michele Lacerenza co-founded PIONIRS s.r.l. aiming to foster novel discoveries and better diagnostics in the medical sector.

Caterina Amendola is a junior researcher specializing in the field of diffuse optics. She serves in the Physics Department of Politecnico di Milano, Italy, where she earned her PhD in March 2022. Her research primarily focuses on time-domain near-infrared spectroscopy (TD-NIRS) and diffuse correlation spectroscopy (DCS) techniques. With expertise in developing hybrid TD-NIRS and DCS devices, she applies these advancements in clinical settings while conducting data analysis and physical modeling.

Mauro Buttafava is the co-founder and CEO at PIONIRS s.r.l, Italy. He graduated in electronics engineering and received his PhD in information technology from Politecnico di Milano. His expertise involves the development of innovative devices for research and biomedical fields: optical spectroscopy and oximetry fluorescence microscopy. He is the co-author of more than 60 publications in journals and conference proceedings and two patents. In 2020, he co-founded PIONIRS, the first company in the EU to commercialize instrumentation for time-domain NIRS.

Davide Contini received his MS degree in electronic engineering and his PhD in physics from Politecnico di Milano, Italy, in 2004 and 2007, respectively. He is an associate professor in the Department of Physics, Politecnico di Milano. He has authored more than 150 papers in international peer-reviewed journals and conference proceedings. His research activity is focused on time-resolved spectroscopy of highly diffusive media for applications in biology and medicine.

Virginia Rossi graduated with honors in medicine and surgery from the University of Pavia (Italy) in 2019. She is currently a pediatric resident at Buzzi Children's Hospital in Milan, Italy, and is in her fourth year out of a 5-year program. She has authored 27 papers in international peer-reviewed journals and has participated in three projects, both national and international. Her research primarily focuses on pediatric endocrinological diseases, childhood obesity, cardio-metabolic complications related to obesity, telemedicine, and health systems.

Lorenzo Spinelli received his MS and PhD degrees in physics from the University of Milan, Italy, in 1994 and 1999, respectively. He devoted his activity research to the study of structures developing in the section of broad area radiation beams. In 2001, he became a researcher for the Italian Research National Council at the Politecnico of Milan. His current research interest is the study of photon migration in turbid media for optical biopsy and imaging.

Sara Zanelli received her master's degree in medicine and surgery from the University of Pavia, Italy, in 2023 after obtaining a high school scientific diploma. Currently, she has a fellowship at Buzzi Hospital (Milan, Italy) in the Pediatric Unit. She collaborates in research activities in the field of pediatric endocrinology. She is the co-author of five papers.

Gianvincenzo Zuccotti is a full-time professor of pediatrics at the University of Milano, Italy, and the head of the Department of Pediatrics, Vittore Buzzi Children's Hospital, Milan, Italy. He is the author of more than 600 papers in international peer-reviewed journals. He participated in over 80 national and international projects. The main fields of his research have been general and

specialized pediatrics, pediatric infectious diseases, nutrition and malnutrition-related disorders, neonatology, preventive and translational medicine, telemedicine, and health systems.

Alessandro Torricelli is a full-time professor in the Department of Physics, Politecnico di Milan, Italy. He received his MS degree in electronic engineering from Politecnico di Milano in 1994 and his PhD in physics from Politecnico di Torino, Italy, in 1999. He is the author of more than 200 papers in international peer-reviewed journals. His current research interests include photon migration in diffusive media, functional near-infrared spectroscopy, and noninvasive diffuse spectroscopy with time-domain systems.